Received: 10 June 2022 | Revised: 12 August 2022 | Accepted: 22 August 2022

DOI: 10.1002/hyp.14689

RESEARCH ARTICLE

WILEY

Use of geostatistical models to evaluate landscape and stream network controls on post-fire stream nitrate concentrations

Allison E. Rhea[1] | Timothy P. Covino[2] | Charles C. Rhoades[3] | Alexander C. Brooks[1]

[1]Department of Ecosystem Science and Sustainability, Colorado State University, Fort Collins, Colorado, USA

[2]Department of Land Resources and Environmental Studies, Montana State University, Bozeman, Montana, USA

[3]Rocky Mountain Research Station, US Forest Service, Fort Collins, Colorado, USA

Correspondence
Allison E. Rhea, Department of Ecosystem Science and Sustainability, Colorado State University, Fort Collins, CO, USA.
Email: Allison.Rhea@colostate.edu

Funding information
Joint Fire Sciences Program, Grant/Award Number: JFSP# 14-1-06-11; NASA Earth and Space Science Fellowship; National Science Foundation, Grant/Award Numbers: EAR 1642368, EAR 1945504; US Forest Service National Fire Plan, Grant/Award Number: 2016-2019

Abstract

Forested watersheds provide many ecosystem services, such as the filtration of sediment, pollutants, and nutrients, which are increasingly threatened by wildfire. For example, stream nutrient concentrations often increase following wildfire and can remain elevated for decades, making downstream waters susceptible to eutrophication. We investigated the drivers of persistent elevated stream nutrients, specifically nitrate (NO_3^-), in nine watersheds that were burned 16 years prior by the Hayman fire, Colorado, USA. We evaluated the ability of multiple linear regression and spatial stream network modeling approaches to predict observed concentrations of the biologically active solute NO_3^- and the conservative solute sodium (Na^+) which serves as a partial control. Specifically, we quantified the degree to which landscape and stream network characteristics predict stream solute concentrations. Stream Na^+ exhibited strong spatial autocorrelation that was primarily controlled by topography and hydrology. In contrast, stream NO_3^- had higher spatial variability and was inversely correlated to vegetation cover, measured as mean normalized differenced moisture index (NDMI). Spatially heterogeneous wildfire behaviour left intact forest patches interspersed with high burn severity patches dominated by shrubs and grasses which contributes to the spatial variability in stream NO_3^- concentrations. Post-fire vegetation also interacts with watershed structure to influence stream NO_3^- patterns. For example, severely burned convergent hillslopes in headwaters positions were associated with the highest stream NO_3^- concentrations due to the high proportional influence of hillslope water in these locations. Our findings suggest that targeted reforestation in severely burned convergent hillslopes in headwater positions may enhance the recovery of stream NO_3^- concentrations to pre-fire levels.

KEYWORDS
geostatistics, watershed modeling, stream nitrate, wildfire, vegetation recovery, watershed structure

1 | INTRODUCTION

Wildfires are a natural part of many forested ecosystems, but the frequency and severity of wildfires has been increasing across the Western US (Abatzoglou et al., 2017; Westerling, 2016). Elevated wildfire activity can threaten the function of critical forested watersheds that supply fresh water to much of the Western US (Brown et al., 2008). One such example is an increase in nitrogen (N) export post-fire. N typically limits plant growth so N export often indicates ecosystem disturbance and shifts in nutrient supply and demand (Chapin et al., 2011). This net change may increase the potential for eutrophication and harmful algal blooms (Dodds & Smith, 2016; Smith et al., 2011), degrade water treatability (Emelko et al., 2011), and limit terrestrial ecosystem productivity (DeBano, 1991). Short-term (<5 years) increases in stream nitrate (NO_3^-) concentrations have been documented following wildfires across the Western US (Rust et al., 2018; Smith et al., 2011) due to elevated soil N mineralization and leaching (Smithwick et al., 2009; Turner et al., 2007; Wan et al., 2001). In some cases, stream NO_3^- concentrations can remain elevated for decades, particularly in watersheds with a high burn extent and low post-fire vegetation cover (Rhoades et al., 2019; Rust et al., 2019). These results suggest that a lack of vegetation recovery is likely a dominant driver of persistent post-fire NO_3^- export, but this relationship remains poorly understood because vegetation cover, watershed structure, and stream network geometry interact to regulate watershed solute export (Abbott et al., 2021; Covino et al., 2021; Creed & Beall, 2009; Likens & Bormann, 1974; Lovett et al., 2002; Shogren et al., 2021; Zarnetske et al., 2018). Watershed structure is the spatial arrangement of divergent and convergent hillslopes across the landscape (Baiamonte & Singh, 2016; Jencso et al., 2010). Divergent hillslopes are convex and contribute little flow to the stream, whereas convergent hillslopes concentrate hydrologic flowpaths and contribute large inputs to channel networks (Detty & McGuire, 2010). In headwater positions, water and solutes are primarily derived from shallow groundwater contributions from adjacent hillslopes (Covino et al., 2021; Gomi et al., 2002; Likens & Bormann, 1974) whereas upstream sources increasingly dominate water composition in lower network positions (Vannote et al., 1980). Therefore, headwaters are particularly sensitive to disturbance in the surrounding uplands (Lowe & Likens, 2005) and contributions to the stream in these locations have the potential to exert strong control on downstream solute concentrations (Abbott et al., 2018; Alexander et al., 2007; Wohl, 2017).

To better understand the spatial patterns in post-fire water chemistry, we consider both conservative and reactive solutes across a gradient of burn severities and extents. Conservative solutes, such as sodium (Na^+), have low biological demand (Dingman, 2015; Stream Solute Workshop, 1990) and thus concentrations across stream networks are primarily driven by physical transport processes (Webster & Valett, 2006) and watershed geophysical properties (Brennan et al., 2016; French et al., 2020; McGuire et al., 2014). Thus, we can use this conservative solute to represent watershed hydrology. Furthermore, Na^+ is generally not a water quality concern and did not increase after the Hayman Fire (Rhoades et al., 2011). In contrast, concentration patterns of biologically active solutes such as NO_3^- are controlled by interactions between hydrologic transport and biological uptake (Bernhardt et al., 2003, 2005; Gardner & McGlynn, 2009). In particular, forest cover can be a primary control on NO_3^- export at the watershed scale (Bormann & Likens, 1967; Likens et al., 1970). Furthermore, our spatially distributed sampling design characterizes current conditions across watersheds with a gradient of burn severities and extents rather than restricted comparisons of burned and unburned end members that are common in post-fire literature. This allows us to investigate how heterogeneous fire behaviour and watershed structure interact to drive spatial patterns water chemistry.

Statistical models can be used to partition the spatial variance in stream Na^+ and NO_3^- concentrations among landscape (i.e., topographic, vegetation, and fire predictors) and stream network (i.e., flow-connected distance) characteristics. Multiple linear regression (MLR) modeling can be used to determine the relative influence of specific landscape characteristics on spatially distributed solute concentrations (Cho & Lee, 2018; McManus et al., 2020), but this approach assumes independence of sampling locations. Geostatistical modeling approaches, such as spatial stream network (SSN) models, are better suited to differentiate landscape from stream network attributes since they account for spatial autocorrelation of flow-connected samples and the dendritic and unidirectional nature of stream networks (Isaak et al., 2014; Peterson & Ver Hoef, 2010; Ver Hoef et al., 2014). Furthermore, this geostatistical approach facilitates the prediction of water chemistry at unsampled locations through entire stream networks. We paired spatially distributed water chemistry sampling with terrain analysis and vegetation and fire mapping to address the following objectives: (1) examine the degree to which topographic, vegetation, and fire variables predict stream Na^+ and NO_3^- across spatial scales within small headwater networks and (2) evaluate the performance of MLR and SSN models in predicting stream solute concentrations. To our knowledge, this study is the first to use stream geostatistical models to investigate the drivers of elevated post-fire stream NO_3^- concentrations and therefore serves as a useful framework for future work on other fires and water chemistry concerns.

2 | MATERIALS AND METHODS

2.1 | Site description

In 2002, the Hayman Fire burned more than 554 km^2 of ponderosa pine (*Pinus ponderosa*) and Douglas-Fir (*Pseudotsuga menziesii*) forest in the mountainous terrain of the Pike San Isabel National Forest (Graham, 2003) (Figure 1). This was one of the largest wildfires in Colorado's recorded history and 35% of the fire burned at high severity (Robichaud et al., 2003). The fire burned the area contributing to Cheesman Reservoir, a primary drinking water supply to the city of Denver (Graham, 2003). In combination, the 2002 Hayman and 1996 Buffalo Creek fires cost Denver's public water utility tens of millions

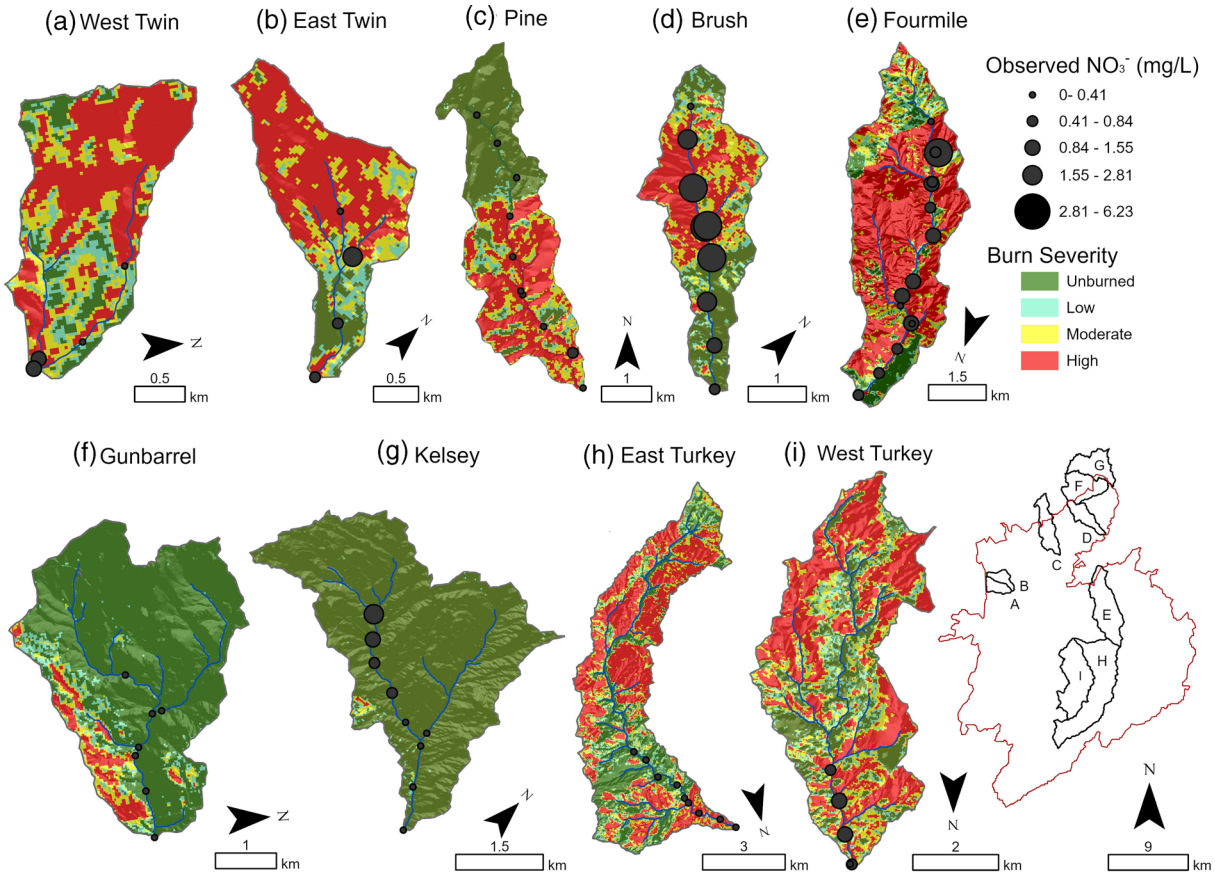

FIGURE 1 Sampling locations within the study watersheds affected by the 2002 Hayman Fire, Colorado, USA. The Hayman fire perimeter is outlined in red in the bottom right with individual watersheds outlined in black and labeled with the associated panel letter. Water chemistry samples ($n = 71$) were collected in June 2018 and the symbol size of each sampling point increases with observed stream NO_3^- concentration

of dollars on water treatment, sediment and debris removal, and reclamation (Hall, 2017). Watersheds within the Hayman Fire burn perimeter receive an annual average of 40 cm of precipitation (WRCC, 2021) and 60%–75% of that comes from summer monsoonal rains (Wilson et al., 2018). Mean elevation within the fire perimeter is 2462 m which is within the intermittent snow zone that does not maintain snow cover throughout the winter (Richer et al., 2013). The parent material underlying our study area is dominated by Pike's Peak Formation granite (Ruleman et al., 2011) which weathers to form coarse, sandy loam soils (Cipra et al., 2003). Ambient Na^+ concentrations are relatively low in granitic basins in our study area. There were no reported post-fire increases in stream Na^+ and measured post-fire increases in other geochemical ions (i.e., calcium, acid neutralizing capacity, and conductivity) recovered to pre-fire levels 2 years after the Hayman Fire (Rhoades et al., 2011).

2.2 | Stream sampling

To quantify the spatial variability of post-fire stream Na^+ and NO_3^- concentrations across a range of burn patterns and severity, we sampled stream water roughly every 800 meters along the mainstems of our study watersheds (Figure 1). This distance was selected to ensure a consistent sampling interval that maximized the number of samples collected per watershed but would allow us to complete watershed sampling within one day. Low-flow conditions were stable and there were no precipitation events during our sampling period (6/1/2018–6/7/2018). Previous research at the Hayman Fire demonstrated that patterns of elevated stream NO_3^- in severely burned watersheds persist across flow conditions (Rhoades et al., 2019) so our June sampling period should be broadly representative. All stream samples from a given watershed were collected within a single day in pre-washed 1 L high-density polyethylene bottles moving in the upstream direction. Samples were immediately filtered with 0.45 μm polyvinyl diethylene filters (MilliporeSigma, Burlington, MA) and analysed for concentrations of stream Na^+ and NO_3^- using ion chromatography (Dionex ICS-3000, Waltham, MA and Waters 580, Sunnyvale, CA). Detection limits for both Na^+ and NO_3^- were 0.01 mg/L and any concentrations below that were replaced with ½ the detection limit.

2.3 | Geospatial analysis

We conducted a terrain analysis to characterize the underlying watershed structure. First, flow direction was derived from a 10-m digital elevation model (DEM) (U.S. Geological Survey, 2018) using the

multiple triangular flow direction algorithm (Seibert & McGlynn, 2007). Watershed contributing areas were delineated and calculated for all sampling points (0.32–35.4 km^2) using the openSTARS package (Peterson & Ver Hoef, 2014) in R Studio. We summarized topographic, vegetation, and fire variables as means and proportional extents within the contributing areas for each sampling location (Table 2) using the SSN package (Ver Hoef et al., 2014).

Topographic metrics included contributing area, mean slope, mean elevation, riparian extent, and mean topographic wetness index (TWI) (Table 1). Slope, elevation, and TWI were derived from the 10-m DEM using Whitebox tools (Lindsay, 2020; Wu, 2021) and summarized as watershed means (Table). TWI serves as a static measure of wetness (i.e., soil and shallow sub-surface moisture) throughout a watershed based on topographic features such as local upslope accumulated area and slope angle (Beven & Kirkby, 1979) (Formula (1)).

$$\mathrm{TWI} = \ln \frac{\alpha}{\tan(\beta)}, \tag{1}$$

where α is the incremental increase in contributing area per unit contour length and β is the local slope. We used a physical definition of the riparian corridor that included pixels <2 m above the stream surface elevation (*sensu* Jencso et al., 2010) and calculated riparian extent as the total riparian corridor area divided by contributing area of each sampling point. This approach differs from an earlier estimate of the extent of riparian vegetation in these watersheds (Rhoades et al., 2019).

We characterized vegetation condition using three spectral indices—normalized differenced vegetation index (NDVI), enhanced vegetation index (EVI), and normalized differenced moisture index (NDMI)—which utilize different wavelengths and therefore have distinct sensitivities to the structural conditions of forests (Pickell et al., 2016). NDVI is the most common index that uses near-infrared (NIR) and Red bands which are sensitive to changes in foliar condition (i.e., green leaf area and biomass) (Formula (2)).

$$\mathrm{NDVI} = \frac{(\mathrm{NIR} - \mathrm{Red})}{(\mathrm{NIR} + \mathrm{Red})}. \tag{2}$$

EVI is a derivative of NDVI that has improved sensitivity in high biomass regions through the integration of the blue band (Formula (3)).

$$\mathrm{EVI} = 2.5 \times \frac{(\mathrm{NIR} - \mathrm{Red})}{(\mathrm{NIR} + 6 \times \mathrm{Red} - 7.5 \times \mathrm{Blue} + 1)}. \tag{3}$$

NDVI and EVI characterize foliage, rather than vegetation structure so they recover to pre-fire levels relatively quickly as grasses and forbs quickly colonize disturbed sites (Buma, 2012; Schroeder et al., 2011). However, spectral indices with longer wavelengths, such as short wave infrared (SWIR), can be more sensitive to forest change and recovery (Schroeder et al., 2011). NDMI utilizes both NIR and SWIR, allowing it to characterize canopy cover and vegetation water stress (Formula (4)).

$$\mathrm{NDMI} = \frac{(\mathrm{NIR} - \mathrm{SWIR})}{(\mathrm{NIR} + \mathrm{SWIR})}. \tag{4}$$

Accordingly, NDMI is more sensitive to forest loss and recovery than NDVI which is broadly sensitive to the amount of photosynthetically active vegetation and post-disturbance NDMI recovery is generally

TABLE 1 Summary of watershed predictor variables and their correlation with observed water chemistry

				Correlation coefficient	
	Variable	Summary statistic	Data source	Na^+	NO_3^-
Topographic	Contributing area	Value at sampling point	Whitebox flow accumulation tool	0.12	−0.03
	Slope	Watershed mean	Whitebox slope tool	0.27	−0.32
	Elevation	Watershed mean	10-m digital elevation model	−0.23	−0.27
	Riparian extent	% of contributing area	Whitebox elevation above stream tool	0.24	−0.01
	TWI	Watershed mean	Whitebox twi tool	−0.33	0.14
Vegetation	Tree cover	Watershed mean	Rangeland analysis platform	0.15	−0.5
	Shrub cover	Watershed mean	Rangeland analysis platform	−0.24	0.15
	Bare cover[x]	Watershed mean	Rangeland analysis platform	−0.12	0.44
	NDMI	Watershed mean	Climate engine	0.09	−0.67
	NDVI[x]	Watershed mean	Climate engine	0.05	−0.64
	EVI[x]	Watershed mean	Climate engine	−0.02	−0.62
Fire	Burn extent	% of contributing area	MTBS	−0.24	0.43
	dNBR[x]	Watershed mean	MTBS	−0.26	0.37

Note: Pearson correlation coefficients were calculated between each predictor variable and Na^+ or NO_3^-. Vegetation metrics represent current conditions (i.e., June 2018) whereas fire metrics represent immediate post-fire condition (i.e., August 2003). Variables marked with a [x] were removed prior to linear mixed model selection due to strong correlation (>0.90) with another predictor variable.

Abbreviations: dNBR, differenced normalized burn ratio; EVI, enhanced vegetation index; MTBS, monitoring trends in burn severity database; NDMI, normalized differenced moisture index; NDVI, normalized differenced vegetation index; TWI, topographic wetness index.

TABLE 2 Physical characteristics and solute concentrations of each study watershed for samples collected in June 2018

	Physical characteristics				Solute concentrations			
					NO_3^-		Na^+	
Watershed	Contributing area (km^2)	Mean slope (%)	Mean elev. (m)	Mean NDMI ( )	Mean (cv) (mg/L)	Min–Max (mg/L)	Mean (cv) (mg/L)	Min–Max (mg/L)
Fourmile	18.8	26	2441	−0.11	1.14 (1.28)	0.17–6.23	6.38 (0.26)	4.95–10.88
East Twin	3.2	30	2640	−0.06	0.88 (1.07)	0.005–2.21	6.46 (0.08)	5.77–6.91
West Twin	3.3	38	2694	−0.05	0.55 (0.88)	0.08–0.97	7.61 (0.15)	6.13–8.8
West Turkey	22	25	2523	−0.08	0.88 (0.22)	0.71–1.07	7.73 (0.01)	7.68–7.82
East Turkey	35.4	17	2571	−0.08	0.29 (0.23)	0.19–0.38	6.78 (0.03)	6.48–7.13
Brush	6.1	28	2277	−0.13	3.06 (0.65)	0.28–5.63	6.23 (0.42)	4.71–12.96
Pine	9.3	35	2516	−0.06	0.23 (0.80)	0.005–0.63	8.40 (0.36)	3.89–13.11
Gunbarrel	12.3	27	2361	−0.02	0.16 (0.66)	0.03–0.30	7.80 (0.07)	6.74–8.18
Kelsey	12.1	22	2284	−0.04	0.56 (1.06)	0.01–1.92	8.94 (0.11)	7.56–10.86

Note: NDMI is the average normalized differenced moisture index in June 2018, and cv is the coefficient of variation.

slower than NDVI (Cuevas-González et al., 2009; Morresi et al., 2019; Pickell et al., 2016; Schroeder et al., 2011). We obtained mean June 2018 vegetation indices from Landsat using Climate Engine (Huntington et al., 2017) to match the vegetation characterization with the timing of our stream sampling. We also included fractional land cover estimates derived from 2018 satellite imagery that was extensively calibrated across the Western US and estimated the proportion of each Landsat pixel covered by trees, shrubs, and bare ground (Allred et al., 2021).

Mean differenced normalized burn ratio (dNBR, a measure of burn severity) and burn extent were calculated for the area contributing to each sampling point. These fire metrics represent immediate post-fire impacts by differencing one pre-fire (8/24/2001) and one post-fire (8/14/2003) Landsat image. dNBR was then classified into categorical burn severity as follows: −150–140 unburned; 140–211 low severity; 211–350 moderate severity, 350–953 high severity (Eidenshink et al., 2009). Low severity fire tends to leave tree canopies largely unaltered whereas high severity fire typically causes complete consumption of surface organic matter and canopy foliage (Parsons et al., 2010). Wildfire severity varies spatially across topographic, vegetation (i.e., fuel composition, arrangement, condition), and weather gradients (Taylor et al., 2021) which creates mosaics of post-fire vegetation structure and composition that vary at scales finer than mapped severity patches (Lentile et al., 2007). To characterize the spatial burn patterning of each watershed, we calculated burn extent, patch size, patch radius, and patch density by severity (Table 3). Burn extent reflects the proportion of contributing area that was burned by each severity class. All patch metrics were calculated with the landscape metrics package (Hesselbarth et al., 2019) in R Studio which defines contiguous cells belonging to the same burn severity class. For each watershed, we determined patch area and calculated patch radius as the mean distance from each cell in a patch to its centroid, and patch density as the number of patches divided by contributing area.

2.4 | Statistical modeling

We used statistical models to evaluate the degree to which topographic, vegetation, and fire variables and flow-connected distance control post-fire stream water chemistry – specifically, concentrations of Na^+ and NO_3^-. Concentration data were log-transformed to improve normality and a correlation analysis removed redundant predictor variables with a correlation >0.90 (Figure 2, Table 1). To identify the top-performing Na^+ and NO_3^- models, we went through a two-step model selection process (*sensu* McManus et al., 2020; Rodríguez-González et al., 2019). First, we identified which landscape characteristics best predicted stream Na^+ and NO_3^- using linear mixed model selection which tested every linear combination of predictor variables while including a random watershed variable to account for the nested sampling design (Table S1). The Na^+ and NO_3^- models with the lowest maximum likelihood estimate of Akaike's Information Criteria (AIC) then progressed to the second phase of model selection where we compared the effect of spatial autocorrelation on model results. We initially ran multiple linear regression (MLR) models which use landscape characteristics to predict observed water chemistry at each sampling location. The predictor variables are spatially explicit given that they characterize the area contributing to a specific sampling point, but MLR models assume independence between stream water samples. We then compared MLR models to spatial stream network (SSN) models that jointly consider landscape and stream network characteristics. This approach captures spatial effects beyond those directly attributable to predictor variables by accounting for flow-connection and using an autocovariance function to account for spatial structure in residual errors (Isaak et al., 2014). MLR and SSN model performance was compared through iterative leave-one-out cross-validation. Observations at sampling points were removed one at a time and the model was used to predict each of the removed values along with the prediction standard error (Ver Hoef & Peterson, 2020). The model with the lowest AIC and root mean

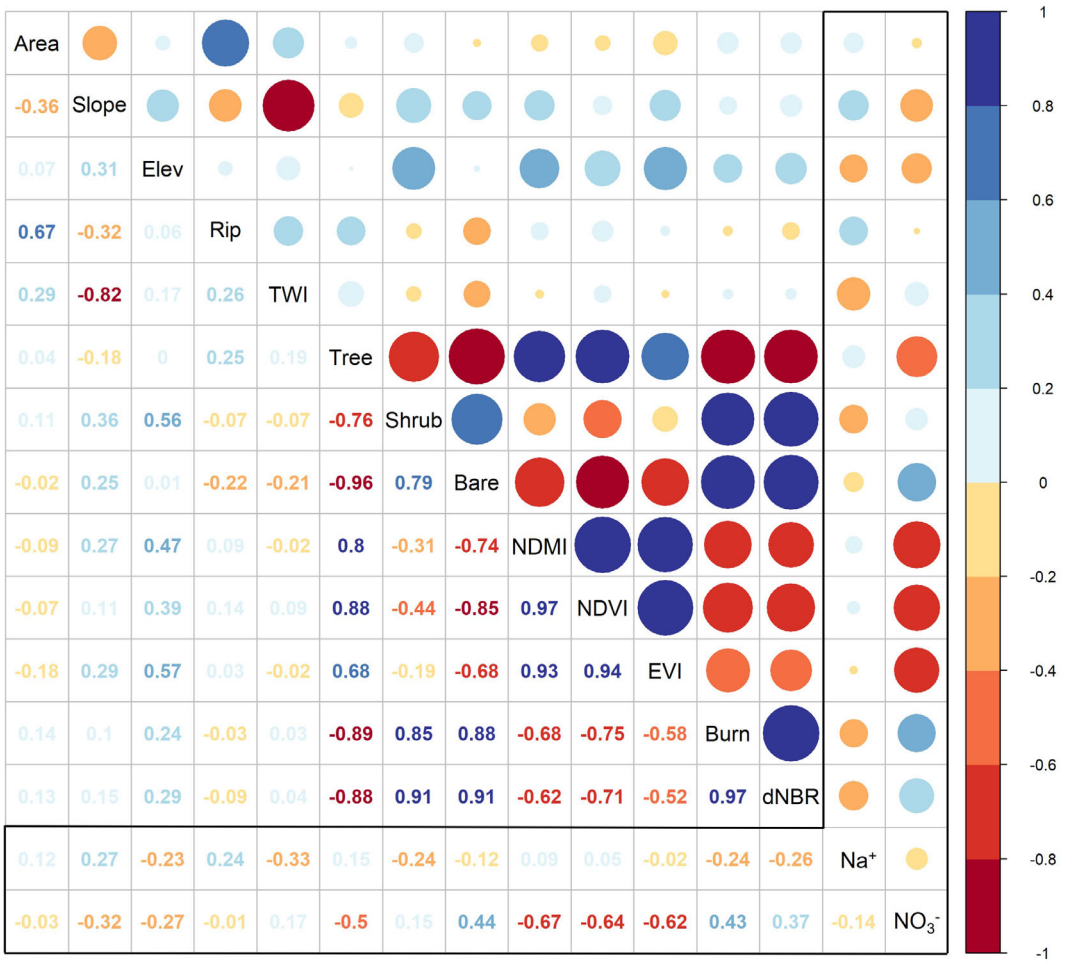

FIGURE 2 Pearson correlation matrix between all potential predictor and response variables. The black box highlights correlations between the predictor variables and stream Na^+ and NO_3^-, both of which were log-transformed. Everything beyond the black box represents correlations among predictor variables. Area is contributing area, Slope is mean watershed slope, Elev is mean watershed elevation, Rip is riparian extent, TWI is mean topographic wetness index, Tree is mean tree cover (%), Shrub is mean shrub cover (%), Bare is mean bare ground cover (%), NDMI is mean normalized differenced moisture index, NDVI is mean normalized differenced vegetation index, EVI is mean enhanced vegetation index, Burn is burn extent (%), and dNBR is mean differenced normalized burn ratio

square prediction error (RMSPE) was selected for use in predictive mapping of stream solute concentrations.

We used the openSTARS (Kattwinkel & Szöcs, 2020) and SSN packages (Ver Hoef et al., 2014) to build the SSN models. First, stream sampling locations were incorporated into a landscape network (LSN) to characterize network geometry (Peterson & Ver Hoef, 2014). The additive function quantified the proportional influence of each stream segment (Ver Hoef & Peterson, 2020) and calculated distance matrices between all sampling points. We used a tail-up autocovariance structure to restrict our modeling to flow-connected distance, which is only measured between points with an upstream-to-downstream connection (Isaak et al., 2014; Peterson & Ver Hoef, 2010). This distance metric is better suited for stream network studies than straight-line Euclidean distance because it characterizes downstream transport and longitudinal connectivity of dissolved solutes (Peterson & Ver Hoef, 2010). We then compared empirical semivariograms with spherical and exponential fits, selected the best-performing structure (i.e., lowest AIC), and used the modeled distribution to derive three associated parameters—the nugget, sill, and range. Empirical semivariograms quantify the variation between samples (i.e., stream Na^+ or NO_3^- concentrations) as a function of distance between sampling points (Ganio et al., 2005). Positive autocorrelation occurs when semivariance is smaller (i.e., measurements are more similar) near the origin and increases at greater lag distances. In some cases, the semivariogram will reach an inflection point at a given lag distance ('range') where semivariance begins to flatten out ('sill'). Samples are considered uncorrelated at distances greater than the range and the sill represents the dissimilarity of the uncorrelated data (Isaak et al., 2014). The nugget describes spatial variation at scales smaller than the minimum sampling interval (i.e., ≤52 m in our study).

2.5 | Longitudinal patterns across two watersheds with inverse spatial burn patterns

Finally, we used the SSN package in R (Ver Hoef et al., 2014) to interpolate stream NO_3^- concentrations along the mainstems of two paired

TABLE 3 Burn metrics by severity for each study watershed. These metrics represent immediate fire impacts by differencing one pre-fire (8/24/2001) and one post-fire (8/14/2003) Landsat image and severity is classified according to MTBS thresholds (Eidenshink et al., 2009)

	Burn extent			Mean patch size / Mean patch radius				
Watershed	Low (%)	Moderate (%)	High (%)	Unburned (ha/m)	Low (ha/m)	Moderate (ha/m)	High (ha/m)	Patch density (#/100 ha)
Fourmile	8	17	64	2/29	1/22	1/32	18 /53	42
East Twin	10	22	57	1/21	1/23	1/38	13/63	44
West Twin	12	26	51	1/39	1/27	1/42	10/73	56
West Turkey	13	20	46	3/41	0/23	1/37	11/67	59
East Turkey	12	17	45	4/37	0/23	1/34	11/72	56
Brush	11	23	38	4/40	0/23	2/41	8/49	50
Pine	7	16	36	8/43	0/20	1/40	21/98	31
Gunbarrel	6	6	6	73/130	0/20	1/28	5/79	24
Kelsey	1	0	0	597/758	0/8	1/26	1/72	6

watersheds and compared spatial NO_3^- patterns to continuous measures (i.e., every 10 m) of hydrologic inputs and the vegetation condition of those inputs. These two watersheds had similar total contributing areas (6.1 and 9.3 km^2, Table 1) and were extensively burned (i.e., >50% of contributing area burned). For both watersheds, patch density was high and fire severity was mixed equally among burn severity classes (Table 3). However, the headwaters were severely burned in Brush Creek and unburned in Pine Creek (Figure 1). We distributed 3,000 equally spaced prediction points along the geomorphic channel networks of each watershed, delineated the contributing area of each prediction point, and calculated topographic, vegetation, and fire predictor variables (see Section 2.3). We also calculated the flow-connected distance between all observed and prediction locations. The NO_3^- SSN model then predicted NO_3^- concentration and standard error at each location based on both landscape characteristics (i.e., contributing area, riparian extent, mean TWI, and mean NDMI) and flow-connected distance. We then calculated the relative lateral input (LI) as the incremental downstream increase in contributing area relative to the total contributing area (i.e., $\text{Relative LI} = \left(\text{area}_{\text{cell}(n)} - \text{area}_{\text{cell}(n-1)}\right)/\text{area}_{\text{cell}(n)}$). Because stream discharge scales with contributing area (Bergstrom et al., 2016), this metric reflects the proportional increase in contributing area relative to total contributing area at that point. Finally, mean NDMI was calculated for the discrete lateral input (LI) contributing to each 10-m stream cell using the same June 2018 NDMI image described in Section 2.3. We also resampled the paired watersheds in June of 2019 at a 300 m resolution to assess the accuracy of our NO_3^- SSN predictions with observed values.

3 | RESULTS

3.1 | Watershed characteristics and stream Na^+ and NO_3^- concentrations

Our nine study watersheds had contributing areas ranging from 3.2 to 35.4 km^2, slope of the contributing hillslopes ranged from 17–38%, and elevation from 2284 to 2694 m (Table 2). At the time of our sampling, 16 years after the fire, mean normalized differenced moisture index (NDMI) was the lowest in Brush (−0.13) and highest in Gunbarrel (−0.02) where burn extents were 71 and 18% respectively (Tables 2 and 3). Burn extent varied from 1% to 90% across the watersheds, but seven of them had more than half of their contributing area burned and 36%–64% of that burned at high severity (Table 3). Patch density was high which is consistent with a mixture of fire severity classes. High severity fire, defined by complete canopy consumption, generally had the largest patch size and radius (Table 3), suggesting that post-fire pine reestablishment may be limited in high severity areas (Chambers et al., 2016).

Observed stream Na^+ concentrations ranged from 3.9–13.1 mg/L (-Figure S1), with an average concentration of 7.3 mg/L which is similar to the pre-fire average of 6.1 mg/L reported in these granitic basins (Rhoades et al., 2011). Kelsey had the highest and Brush had the lowest mean stream Na^+ concentration whereas Brush had the highest and West Turkey had the lowest coefficient of variation (Table 2). Observed stream NO_3^- concentrations varied by three orders of magnitude (0.005–6.2 mg/L) and average stream NO_3^- concentration was 0.91 mg/L which is five times greater than pre-fire concentrations (0.18 mg/L) (Rhoades et al., 2019). Brush watershed had the highest (3.06 mg/L) and Gunbarrel the lowest (0.16 mg/L) mean NO_3^- concentration whereas Fourmile had the greatest and West Turkey the lowest coefficient of variation (Table 2). The coefficient of variation was consistently higher for stream NO_3^- concentrations (Table 2) indicating greater within-watershed variability in stream NO_3^- compared to Na^+.

Topographic variables had weak correlations (<0.32) with both stream Na^+ and NO_3^- (Table 1). Vegetation predictors generally had much stronger correlations with NO_3^- compared to Na^+, with the exception of shrub cover (Table 1). Burn variables had slightly higher correlations with NO_3^- compared to Na^+ (Table 1). All predictor variables that were selected through linear mixed model selection were weakly correlated with water chemistry (<0.33) (Figure S2). The one exception was a strong inverse relationship between mean NDMI

and stream NO_3^- which had a correlation coefficient of −0.67 (Figure S2).

3.2 | Landscape and stream network controls on Na^+ and NO_3^- concentrations

Vegetation and fire predictor variables were weakly correlated (0.01–0.26) and topographic predictors were more strongly correlated (0.12–0.33) with log[Na^+] (Table 1). Linear mixed model selection identified contributing area, slope, riparian extent, TWI, and tree and shrub cover as the best predictors of log[Na^+] (Table S1). Together, watershed predictors explained 54.4% of the variance in log[Na^+] in the Na^+ MLR model and 45% of the variance in the Na^+ SSN model (Table 4). In the Na^+ SSN model, 53.1% of variation in log[Na^+] was explained by flow-connected autocorrelation (Table 4). Na^+ exhibited strong positive autocorrelation where semivariance was low at short lag distances, but increased with distance (Figure 3). When flow-connected autocovariance was modeled with a spherical fit, Na^+ had a nugget of 0.001, sill of 0.029, and range of 3,700 m (Figure 3). The SSN model improved Na^+ predictions relative to the MLR model, as indicated by lower AIC, RMSPE, and unexplained variance values (61%, 20%, and 96% lower, respectively) (Table 4). This is demonstrated in the leave one-out-cross validation where SSN predictions were closer to observed values (Figure 4a) and prediction standard errors were lower (Figure 4c) in the Na^+ SSN model compared to the Na^+ MLR model.

Fire and vegetation variables generally had stronger correlations (0.15–0.67) with log[NO_3^-] than topographic variables (0.03–0.32) (Table 1). Linear mixed model selection identified contributing area, riparian extent, TWI, and NDMI as the best predictors of log[NO_3^-] (Table S1) and mean NDMI had the strongest correlation with log[NO_3^-] (Figure 2). In the NO_3^- MLR model, the selected predictor variables, with the exception of riparian extent, were significant and accounted for 51.4% of the variance in log[NO_3^-] (Table 4). In the NO_3^- SSN model, TWI and NDMI were the only significant predictor variables and the predictors explained 36% of variation in log[NO_3^-] while flow-connected autocorrelation explained 41.5% of variation in log[NO_3^-] (Table 4). Stream NO_3^- had high semivariance across all flow-connected distances, though semivariance peaked at intermediate lag distances (1,000–5,000 m) (Figure 3). When flow-connected autocovariance was modeled with an exponential fit, NO_3^- had a nugget of 0.385, sill of 0.708, and range of 8800 m which is equal to our maximum sampling distance (Figure 3). The NO_3^- SSN model also had

TABLE 4 Summary of spatial stream network (SSN) and multiple linear regression (MLR) models that predict log-transformed stream Na^+ and NO_3^- concentrations. Parameter estimates represent the regression coefficient, which is the change in the response variable based on a 1-unit change in the predictor variable while holding all other variables constant. Variance decomposition assigns variance in Na^+ or NO_3^- to watershed predictor variables, flow-connected autocorrelation, and unexplained variance. MLR models do not account for flow-connected autocovariance. Model performance metrics come from iterative leave-on-out cross-validation

		Na^+ models		NO_3^- models	
		SSN	MLR	SSN	MLR
Parameter estimates	Contributing area	0.008	0.012**	−0.03	−0.04*
	Slope	0.090***	0.104***	-	-
	Elevation	-	-	-	-
	Riparian extent	0.100**	0.106***	0.32	0.29
	TWI	0.651*	0.813***	1.33*	0.91*
	Tree cover	−0.02***	−0.018***	-	-
	Shrub cover	−0.115***	−0.111***	-	-
	NDMI	-	-	−17.64***	−17.37***
	Burn extent	-	-	-	-
Variance components (%)	Predictor variables	45.0	54.4	36.0	51.4
	Flow-connected distance	53.1	-	41.5	-
	Total explained	98.1	54.4	77.5	51.4
	Unexplained	1.9	45.6	22.5	48.6
Model performance	AIC	−55.35	−34.29	210	212
	RMSPE	0.165	0.205	1.00	1.07

Abbreviations: AIC, Akaike's information criteria; NDMI, normalized difference moisture index; RMSPE, root mean square prediction error; TWI, topographic wetness index.

*Statistical significance of predictor variables = 0.05.

**Statistical significance of predictor variables = 0.01.

***Statistical significance of predictor variables = 0.001.

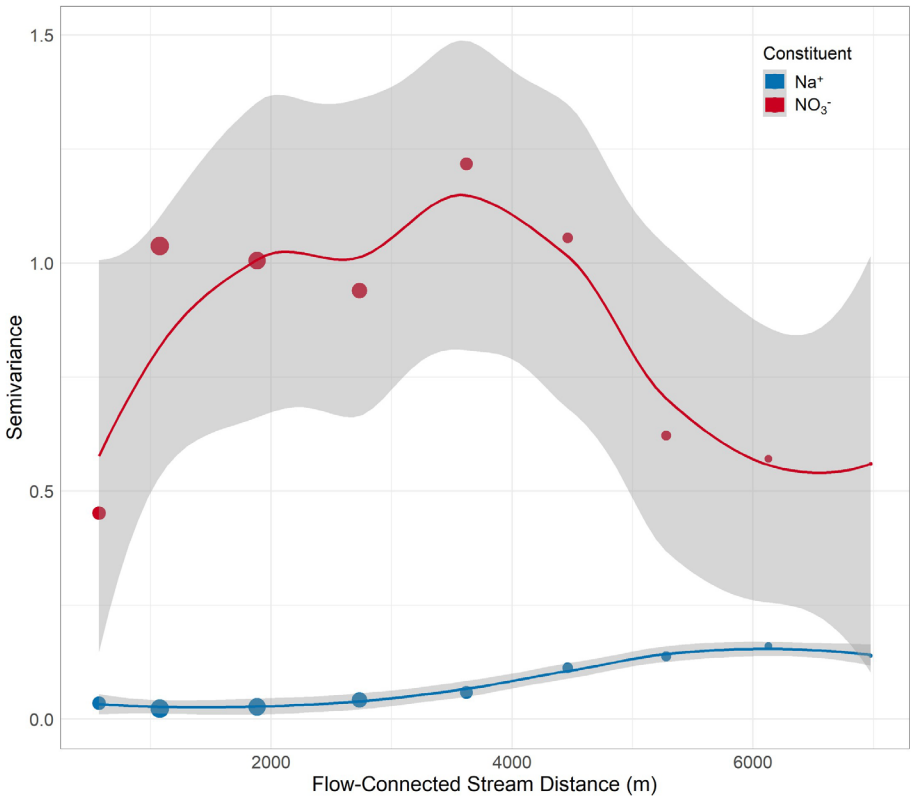

FIGURE 3 Empirical semivariograms of log-transformed stream Na^+ (blue) and NO_3^- (red) based on the flow-connected distance between sampling points. Symbol sizes are proportional to the number of data pairs included in each bin. The grey shaded region represents the 95% confidence interval from a local polynomial regression of each semivariogram. Semivariograms show evidence of strong positive autocorrelation in Na^+ (blue) and weak spatial autocorrelation in NO_3^- (red)

lower AIC, RMSPE, and unexplained variance values relative to the NO_3^- MLR model (<1%, 7%, and 54% lower, respectively) (Table 4). Based on leave-on-out cross validation, SSN predictions were closer to the observed values (Figure 4b) and prediction standard error was lower (Figure 4d) in the NO_3^- SSN model than the MLR model.

3.3 | Longitudinal patterns across two watersheds with inverse spatial burn patterns

The two paired watersheds with inverse burn patterns exhibited strong differences in stream NO_3^- concentration. 72% of Brush Creek watershed was burned and most of the burn occurred in the upper half of the watershed (Figure 5a). Conversely, the majority of the burned area in Pine Creek occurred in the lower half of the watershed (Figure 5b). In Brush Creek, stream NO_3^- concentrations spanned a 4.6 mg/L range. The minimum concentration (0.4 mg/L) occurred at the upper most sampling location and the highest observed concentration (5.0 mg/L) occurred nearby within the upper watershed (Figure 5e). Nitrate generally declined in the lower half of the Brush Creek watershed and reached 0.9 mg/L at the downstream-most sampling location. On the other hand, stream NO_3^- concentrations in Pine Creek increased gradually downstream from below detection levels in the headwaters to 0.3 mg/L at the outlet (Figure 5f). Maximum and mean stream NO_3^- concentrations were 14- and 17-times higher in Brush than Pine Creek. Our NO_3^- SSN model predictions strongly agreed with measured stream NO_3^- concentrations during our 2019 sampling (Figure S3).

4 | DISCUSSION

4.1 | Post-fire vegetation is a dominant driver of stream NO_3^- patterns

The conservative Na^+ and biologically reactive NO_3^- solutes included in this study were controlled by distinct landscape predictor variables. Stream Na^+ concentrations were most strongly correlated with topography (Table 1), which often controls watershed hydrology in mountainous terrain (Bergstrom et al., 2016) whereas correlations between Na^+ and vegetation and fire predictors were relatively weak (Table 1). These observations are consistent with our expectation of low biological demand and strong hydrologic control of conservative Na^+ tracers (Dingman, 2015; Stream Solute Workshop, 1990). In contrast, stream NO_3^- had stronger relationships with vegetation than topographic predictors (Table 1) which supports the understanding that reactive solutes, such as NO_3^-, are more strongly controlled by biotic demand (Bernhardt et al., 2003, 2005; Gardner & McGlynn, 2009). More specifically, spectral vegetation indices were the strongest predictors of stream NO_3^- concentration in this and other studies. For example, reduced post-fire plant cover, measured as NDVI, explained the persistence of elevated post-fire stream N broadly across the Western US (Rust et al., 2019) and earlier work at the Hayman fire demonstrated that stream NO_3^- concentrations were inversely related to riparian vegetation cover (Rhoades et al., 2019). In this study, the strongest predictor of stream NO_3^- concentration was mean NDMI (Figure 2), a vegetation index that considers both canopy cover and the water stress of that vegetation and is particularly sensitive to burn

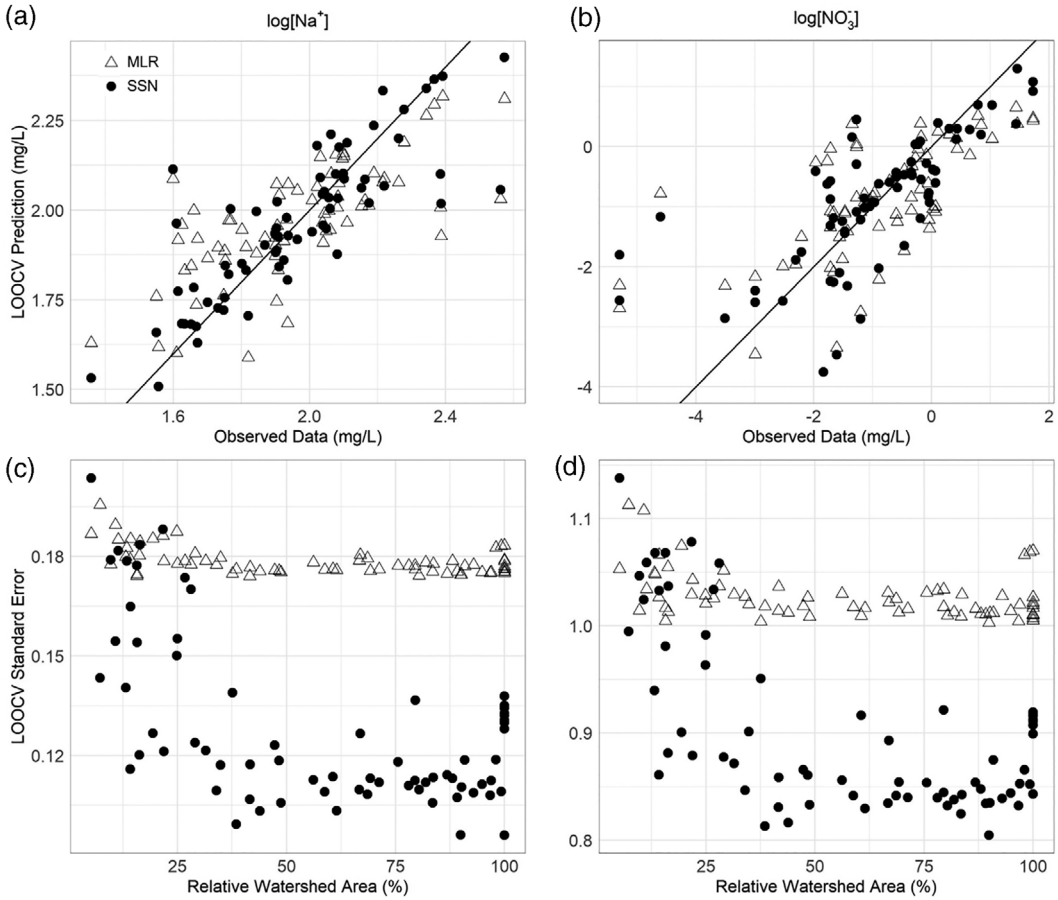

FIGURE 4 Leave-one-out cross validation to assess (a, c) Na^+ and (b, d) NO_3^- model performance. (a–b) Model predictions are plotted against observed values for both MLR (open triangles) and SSN (black circles) models. (c–d) Prediction standard error is plotted against relative upslope accumulated area, with headwater positions on the left side of the plot and lower watershed positions on the right side

severity, forest type, and forest loss and recovery (Morresi et al., 2019). The strong inverse relationship between NDMI and stream NO_3^- demonstrates that water-stressed areas with low canopy cover were associated with elevated stream NO_3^- concentrations.

Large high severity fire has the potential to shift ecosystems from forest to grass and shrubland which can reduce vegetation N retention. Even a decade after the Hayman and other nearby fires, 75% of high burn severity plots had no conifer regeneration and it is possible that forest density will never return to pre-fire levels in these areas (Chambers et al., 2016). This pattern is due, in part, to the spatial extent of high severity fire which had largest patch size of any severity class in our burned watersheds with a mean radius >50 m (Table 3) indicating that the distance to live seed sources will likely constrain conifer regeneration in these areas (Chambers et al., 2016). Beyond our field sites, there is broad evidence of declining post-fire tree regeneration due to increasing climate aridity and fire activity which can shift previously forested systems into alternative stable states dominated by grassland and weedy, herbaceous vegetation types (Coop et al., 2020; Stevens-Rumann et al., 2018; Tepley et al., 2017; Walker et al., 2018). Because forest cover is often a primary mechanism for terrestrial N retention (Dunnette et al., 2014; Vitousek et al., 1979), changes from forest to grass and shrub cover can impact ecosystem N losses (Lovett et al., 2002). For example, conifers will more strongly regulate N cycling than grasses and forbs given their underlying nutrient use efficiencies (Chapman et al., 2006) so patches with little post-fire tree regeneration will likely be leakier with respect to N.

Stream NO_3^- concentrations exhibited higher spatial variability than conservative Na^+ concentrations. Semivariance was greater for stream NO_3^- than Na^+ across all flow-connected distances (Figure 3) which suggests higher variability in stream NO_3^- concentrations across all measured scales (Isaak et al., 2014). Stream NO_3^- also exhibits patchiness at smaller spatial scales than Na^+ as seen by NO_3^- having a larger nugget value and steeper increase in semivariance with lag distance (Figure 3) (Isaak et al., 2014; Zimmerman & Ver Hoef, 2017). Finally, SSN model improvements tend to be smaller where spatial autocorrelation is lower (Isaak et al., 2014) so the relatively small SSN improvements for stream NO_3^- relative to Na^+ indicate weaker spatial structuring in NO_3^- concentrations. Other studies have attributed stream NO_3^- variability to rapid in-stream uptake and processing (McGuire et al., 2014). Nitrate uptake lengths in nearby

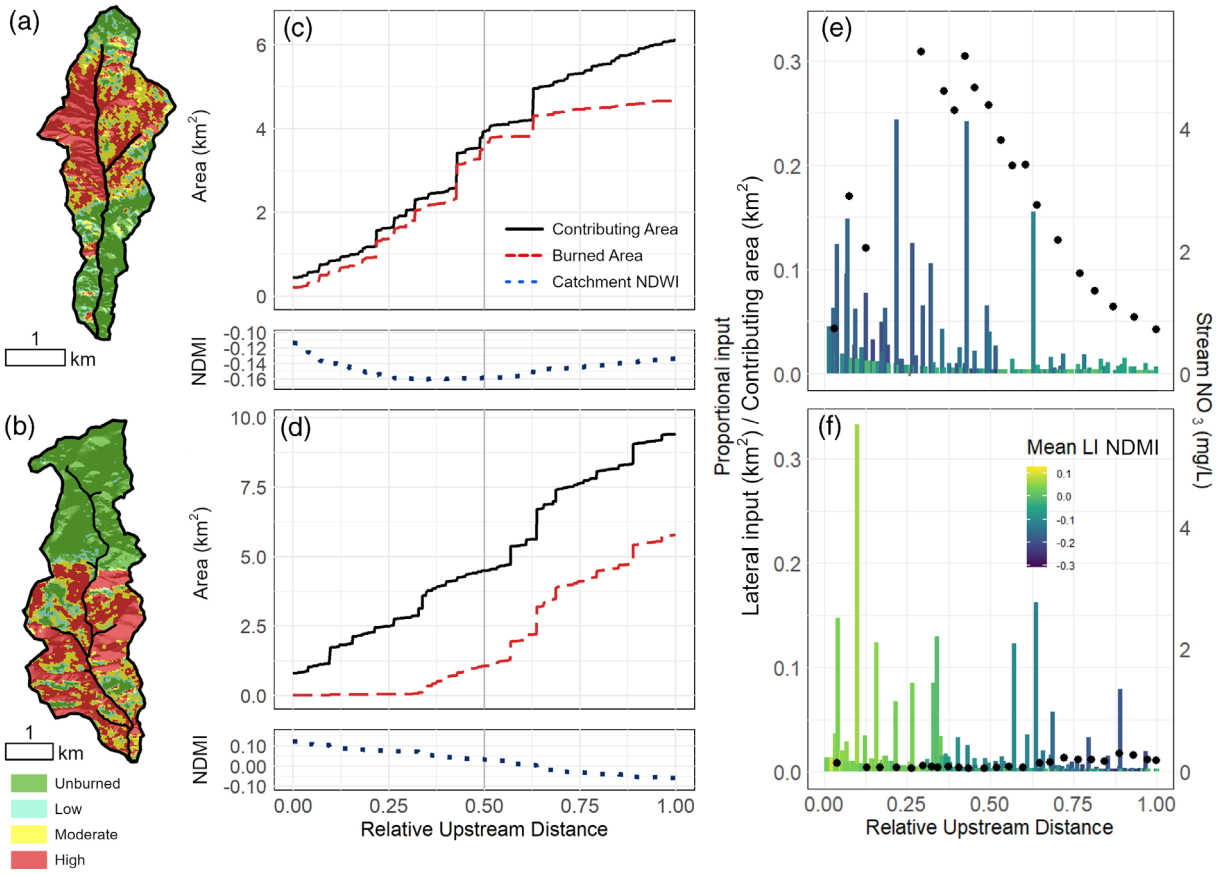

FIGURE 5 Spatial arrangement of burn severity in (a) Brush Creek which was 71% burned with most high severity fire occurring in the upper half of the watershed and (b) Pine Creek which was 59% burned with most high severity fire occurring in the lower half of the watershed. Distribution of cumulative contributing area (black solid lines), cumulative burned area (red dashed lines), and mean catchment NDMI (blue dotted lines) for (c) Brush Creek and (d) Pine Creek. Upstream distance was relativized between 0 and 1 in all plots, with headwaters on the left and outlet on the right, to allow for comparisons between watersheds. The vertical grey line denotes the mid-point of the watershed. Distribution of proportional inputs with upstream distance for (e) Brush Creek and (f) Pine Creek where bars are colored according the mean NDMI of each discrete lateral input. Stream NO_3^- concentrations predicted from the NO_3^- SSN model (black circles) are compared for both (e) Brush Creek and (f) Pine Creek

Wyoming streams ranged from hundreds to thousands of meters (Hall et al., 2009), so uptake is likely to influence NO_3^- patterns across the range of scales in our study (<9,000 m). However, headwater streams with elevated ambient inorganic N concentrations have a limited ability to moderate downstream transport of inorganic N (Covino et al., 2021) because nutrient delivery to streams is often orders of magnitude greater than in-stream production or removal (Brookshire et al., 2009). Our previous work at the Hayman Fire demonstrated that in-stream biotic N demand increased after the fire, but N supply from burned uplands exceeded the increase in stream N demand (Rhea et al., 2021). While in-stream uptake likely contributed to spatial variability in stream NO_3^-, our work demonstrates strong post-fire vegetation controls on the spatial patterns of stream NO_3^- concentrations. Burn severity patch density was high within our study watersheds (Table 3) which is consistent with a mixture of fire severity classes. This results in intact forest patches with high N demand that are interspersed with high burn severity patches that are dominated by shrubs and grasses and have lower N demand. Therefore, spatially variable vegetation N demand likely contributes to the high observed spatial variability in stream NO_3^- concentrations.

4.2 | Burned headwaters are susceptible to elevated stream NO_3^-

Patterns of vegetation cover interact with watershed structure to drive spatial distributions of stream NO_3^- concentrations. In headwater positions, most water and dissolved solutes originate from the surrounding terrestrial landscape, making these areas particularly sensitive to disturbance in the surrounding uplands (Gomi et al., 2002; Likens & Bormann, 1974; Lowe & Likens, 2005). Thus, the vegetation cover of large convergent hillslopes should have stronger proportional influence on stream NO_3^- concentration in headwater positions relative to locations lower in the network. We found that convergent hillslopes in the headwaters of Brush Creek were associated with low NDMI (Figure 5e) and aligned with locations of high stream NO_3^-

(Figure 5e). Additionally, proportional inflows in Brush Creek declined downstream and were associated with higher NDMI. Stream NO_3^- concentrations also declined downstream in Brush Creek, likely due to a combination of reduced proportional influence of hillslope inputs, streamflow dilution, and in-stream N uptake. In the unburned headwaters of Pine Creek, convergent hillslopes were associated with high NDMI (Figure 5f) and likely high terrestrial N demand. Stream NO_3^- concentrations remained low throughout the headwaters of Pine Creek with only slight downstream increases where bur hillslopes were sparsely vegetated (Figure 5f).

This investigation demonstrates that convergent hillslopes in headwater positions are particularly sensitive to wildfire-induced vegetation mortality and can impact both local and downstream water chemistry. Headwater attributes have been shown to predict downstream water chemistry (i.e., NO_3^-, PO_4^{3-}, Ca^{2+}, and Sr^{2+}) at distances exceeding 500 km (French et al., 2020). Our sampled stream networks were 5,520–8,289 m, so headwater attributes could feasibly influence downstream chemistry throughout the entire stream networks. Indeed, the watershed with burned headwaters (i.e., Brush Creek), sustained higher stream NO_3^- concentrations throughout its stream network compared to the watershed with unburned headwaters (i.e., Pine Creek, Figure 5e–f). These findings may help prioritize post-fire watershed rehabilitation efforts aimed at increasing plant cover and nutrient demand to reduce stream NO_3^- concentrations. More specifically, our findings highlight the potential value for post-fire reforestation in convergent headwater locations to enhance N retention and reduce downstream NO_3^- export. This is a first step towards understanding what post-fire restoration strategies are most effective at mitigating lingering post-fire NO_3^- concerns (Rhoades et al., 2019) and should be considered within the context of existing ecological frameworks for post-fire tplanting (Stevens-Rumann & Morgan, 2019).

4.3 | Applications and future research

Our findings help characterize the potential magnitude, duration, and location of water chemistry alteration following fire. Based on kriging from the NO_3^- SSN model, 81% of the predicted stream NO_3^- concentrations that fell within the fire perimeter (Figure S4) exceeded the pre-fire mean concentration of 0.18 mg/L (Rhoades et al., 2011). While the kriging demonstrates that elevated post-fire stream NO_3^- is pervasive throughout the burned landscape 16 years post-fire, it also highlights specific watersheds (e.g., Brush, Fourmile, and West Turkey) and sensitive watershed positions (e.g., tributaries and headwaters) that are experiencing the highest stream NO_3^- concentrations (Figure S4). However, these kriged predictions tend to have the highest standard error in headwaters and tributaries where predictions rely more on watershed attributes than upstream samples (Figure 4c–d). Moving downstream, SSN models are informed by an increasing number of upstream data points and prediction accuracy improves (Figure 4c–d). Therefore, it is critical that post-fire water chemistry sampling extends to headwaters and tributaries where and when possible, in order to maximize kriging accuracy.

The approach presented here could be extended to other wildfires to further investigate the main drivers of post-fire water chemistry, predict water chemistry in unsampled locations, and identify key locations for targeted reforestation. The requisite spatially distributed water sampling can be rapid (i.e., within 1 week in the case of this study), predictor variables are derived from geospatial data sources with extensive temporal and spatial coverage, and the statistical code is publicly available. In particular, this framework would benefit from being applied to a higher order stream network in order to characterize downstream propagation of disturbance signals beyond the small headwater streams captured in our study. However, it is also critical that we move from statistical correlations to field-based experimentation. Future research should monitor natural post-fire vegetation recovery in sensitive watershed positions and assess the capacity for targeted reforestation to retain N and reduce stream NO_3^- concentrations. As slow post-fire regeneration becomes increasingly prevalent in response to higher fire severity and climate aridity (Coop et al., 2020; Stevens-Rumann et al., 2018; Tepley et al., 2017; Walker et al., 2018), such targeted reforestation activities may be critical for the recovery of stream NO_3^- concentrations to pre-fire levels.

5 | CONCLUSIONS

This study utilized spatially distributed water chemistry sampling to identify the controls on stream Na^+ and NO_3^- concentrations across nine post-fire watersheds with varying patterns of burn severity and extent. Statistical modeling was used to partition the variance in stream Na^+ and NO_3^- among landscape (i.e., topographic, vegetation, and fire predictors) and stream network (i.e., flow-connected distance) characteristics. Topographic variables were the strongest predictors of stream Na^+ concentrations and Na^+ exhibited strong positive flow-connected autocorrelation. Together, these results indicate that the spatial distribution of conservative Na^+ concentrations was largely driven by watershed topography and hydrology. In contrast, stream NO_3^- was most strongly correlated with mean NDMI, a metric that characterizes canopy cover and vegetation water stress. Additionally, stream NO_3^- concentrations exhibited high spatial variability across the stream networks. These results suggest that complex patterns of burn severity and extent create a mosaic of unburned forest interspersed with patches of shrubs and grasses that can contribute to high variability in stream NO_3^- concentrations. We also found that sparse forest cover in severely burned convergent hillslopes in headwater positions had a strong impact on local stream NO_3^- concentrations, suggesting that targeted reforestation in these locations may help limit stream NO_3^- concentrations and downstream export.

ACKNOWLEDGEMENTS

We are grateful for financial support from the US Forest Service National Fire Plan (2016-2019) and the Joint Fire Sciences Program (JFSP# 14-1-06-11). A.R. was supported by NASA Headquarters

under the NASA Earth and Space Science Fellowship Program with additional support from NSF award EAR 1642368. T.C.'s time was additionally supported by NSF awards EAR 1945504 and EAR 1642368. Sincere thanks to Tim Fegel of the Rocky Mountain Research Station for his critical contributions to field and laboratory work.

CONFLICT OF INTEREST

The authors declare no conflicts of interest.

DATA AVAILABILITY STATEMENT

The data used in this paper are publicly available through CUASHI HydroShare: Rhea, A. (2022). Use of geostatistical models to evaluate landscape and stream network controls on post-fire stream nitrate concentrations. *HydroShare*. http://www.hydroshare.org/resource/e35a308d4672419c9f75f6897c823c92, reference number e35a308d4672419c9f75f6897c823c92.

ORCID

Allison E. Rhea https://orcid.org/0000-0002-2601-7236
Timothy P. Covino https://orcid.org/0000-0001-7218-4927

REFERENCES

Abatzoglou, J. T., Kolden, C. A., Williams, A. P., Lutz, J. A., & Smith, A. M. S. (2017). Climatic influences on interannual variability in regional burn severity across western US forests. *International Journal of Wildland Fire*, *26*(4), 269–275. https://doi.org/10.1071/WF16165

Abbott, B. W., Gruau, G., Zarnetske, J. P., Moatar, F., Barbe, L., Thomas, Z., Fovet, O., Kolbe, T., Gu, S., Pierson-Wickmann, A. C., Davy, P., & Pinay, G. (2018). Unexpected spatial stability of water chemistry in headwater stream networks. *Ecology Letters*, *21*(2), 296–308. https://doi.org/10.1111/ele.12897

Abbott, B. W., Rocha, A. V., Shogren, A., Zarnetske, J. P., Iannucci, F., Bowden, W. B., Bratsman, S. P., Patch, L., Watts, R., Fulweber, R., Frei, R. J., Huebner, A. M., Ludwig, S. M., Carling, G. T., & O'Donnell, J. A. (2021). Tundra wildfire triggers sustained lateral nutrient loss in Alaskan Arctic. *Global Change Biology*, *27*(7), 1408–1430. https://doi.org/10.1111/gcb.15507

Alexander, R. B., Boyer, E. W., Smith, R. A., Schwarz, G. E., & Moore, R. B. (2007). The role of headwater streams in downstream water quality. *Journal of the American Water Resources Association*, *43*(1), 41–59. https://doi.org/10.1111/j.1752-1688.2007.00005.x

Allred, B. W., Bestelmeyer, B. T., Boyd, C. S., Brown, C., Davies, K. W., Duniway, M. C., Ellsworth, L. M., Erickson, T. A., Fuhlendorf, S. D., Griffiths, T. V., Jansen, V., Jones, M. O., Karl, J., Knight, A., Maestas, J. D., Maynard, J. J., McCord, S. E., Naugle, D. E., Starns, H. D., … Uden, D. R. (2021). Improving Landsat predictions of rangeland fractional cover with multitask learning and uncertainty. *Methods in Ecology and Evolution*, *2021*(January), 1–9. https://doi.org/10.1111/2041-210x.13564

Baiamonte, G., & Singh, V. P. (2016). Overland flow times of concentration for hillslopes of complex topography. *Journal of Irrigation and Drainage Engineering*, *142*(3), 04015059. https://doi.org/10.1061/(asce)ir.1943-4774.0000984

Bergstrom, A., McGlynn, B., Mallard, J., & Covino, T. (2016). Watershed structural influences on the distributions of stream network water and solute travel times under baseflow conditions. *Hydrological Processes*, *30*(15), 2671–2685. https://doi.org/10.1002/hyp.10792

Bernhardt, E. S., Likens, G. E., Buso, D. C., & Driscoll, C. T. (2003). In-stream uptake dampens effects of major forest disturbance on watershed nitrogen export. *Proceedings of the National Academy of Sciences of the United States of America*, *100*(18), 10304–10308. https://doi.org/10.1073/pnas.1233676100

Bernhardt, E. S., Likens, G. E., Hall, R. O., Buso, D. C., Fisher, S. G., Burton, T. M., Meyer, J. L., McDowell, W. H., Mayer, M. S., Bowden, W. B., Findlay, S. E. G., Macneale, K. H., Stelzer, R. S., & Lowe, W. H. (2005). Can't see the forest for the stream? In-stream processing and terrestrial nitrogen exports. *Bioscience*, *55*(3), 219–230. https://doi.org/10.1641/0006-3568(2005)055[0219:acstff]2.0.co;2

Beven, K. J., & Kirkby, M. J. (1979). A physically based, variable contributing area model of basin hydrology. *Hydrological Sciences Bulletin*, *24*(1), 43–69. https://doi.org/10.1080/02626667909491834

Bormann, F. H., & Likens, G. E. (1967). Nutrient cycling. *Science*, *155*(3761), 424–429.

Brennan, S. R., Torgersen, C. E., Hollenbeck, J. P., Fernandez, D. P., Jensen, C. K., & Schindler, D. E. (2016). Dendritic network models: Improving isoscapes and quantifying influence of landscape and in-stream processes on strontium isotopes in rivers. *Geophysical Research Letters*, *43*(10), 5043–5051. https://doi.org/10.1002/2016GL068904

Brookshire, E. N. J., Valett, H. M., & Gerber, S. (2009). Maintenance of terrestrial nutrient loss signatures during in-stream transport. *Ecology*, *90*(2), 293–299.

Brown, T. C., Hobbins, M. T., & Ramirez, J. A. (2008). Spatial distribution of water supply in the coterminous United States. *Journal of the American Water Resources Association*, *44*(6), 1474–1487. https://doi.org/10.1111/j.1752-1688.2008.00252.x

Buma, B. (2012). Evaluating the utility and seasonality of NDVI values for assessing post-disturbance recovery in a subalpine forest. *Environmental Monitoring and Assessment*, *184*(6), 3849–3860. https://doi.org/10.1007/s10661-011-2228-y

Chambers, M. E., Fornwalt, P. J., Malone, S. L., & Battaglia, M. A. (2016). Patterns of conifer regeneration following high severity wildfire in ponderosa pine – Dominated forests of the Colorado Front Range. *Forest Ecology and Management*, *378*, 57–67. https://doi.org/10.1016/j.foreco.2016.07.001

Chapin, F. S., Mooney, H. A., & Matson, P. A. (2011). *Principles of terrestrial ecosystem ecology* (2nd ed.). Springer.

Chapman, S. K., Langley, J. A., Hart, S. C., & Koch, G. W. (2006). Plants actively control nitrogen cycling: Uncorking the microbial bottleneck. *New Phytologist*, *169*(1), 27–34. https://doi.org/10.1111/j.1469-8137.2005.01571.x

Cho, J. H., & Lee, J. H. (2018). Multiple linear regression models for predicting nonpoint-source pollutant discharge from a highland agricultural region. *Water (Switzerland)*, *10*(9), 1–17. https://doi.org/10.3390/w10091156

Cipra, J., Kelly, E., MacDonald, L., & Norman, J. (2003). Soil properties, erosion, and implications for rehabilitation and aquatic ecosystems. In *Hayman Fire case study* (pp. 204–219). https://doi.org/10.2737/RMRS-GTR-115

Coop, J. D., Parks, S. A., Stevens-Rumann, C. S., Crausbay, S. D., Higuera, P. E., Hurteau, M. D., Tepley, A., Whitman, E., Assal, T., Collins, B. M., Davis, K. T., Dobrowski, S., Falk, D. A., Fornwalt, P. J., Fulé, P. Z., Harvey, B. J., Kane, V. R., Littlefield, C. E., Margolis, E. Q., … Rodman, K. C. (2020). Wildfire-driven forest conversion in Western North American landscapes. *Bioscience*, *70*(8), 659–673. https://doi.org/10.1093/biosci/biaa061

Covino, T., Riveros-Iregui, D. A., & Schneider, C. L. (2021). Geomorphology imparts spatial organization on hydrological and biogeochemical fluxes. In *Reference module in earth systems and environmental sciences*. Elsevier Inc. https://doi.org/10.1016/b978-0-12-818234-5.00068-7

Covino, T. P., Wlostowski, A. N., Gooseff, M. N., Wollheim, W. M., & Bowden, W. B. (2021). The seasonality of in-stream nutrient concentrations and uptake in Arctic headwater streams in the northern foothills of Alaska's Brooks Range. *Journal of Geophysical Research: Biogeosciences*, *126*(4), 1–18. https://doi.org/10.1029/2020JG005949

Creed, I. F., & Beall, F. D. (2009). Distributed topographic indicators for predicting nitrogen export from headwater catchments. *Water Resources Research*, *45*(10), 1–12. https://doi.org/10.1029/2008WR007285

Cuevas-González, M., Gerard, F., Balzter, H., & Riaño, D. (2009). Analysing forest recovery after wildfire disturbance in boreal Siberia using remotely sensed vegetation indices. *Global Change Biology*, *15*(3), 561–577. https://doi.org/10.1111/j.1365-2486.2008.01784.x

DeBano, L. F. (1991). The effect of fire on soil properties. In A. E. Harvey & L. F. Neuenschwander (Eds.), *Proceedings management and productivity of Western-Montane forest soils* (pp. 151–156). https://doi.org/10.2737/INT-GTR-280

Detty, J. M., & McGuire, K. J. (2010). Topographic controls on shallow groundwater dynamics: Implications of hydrologic connectivity between hillslopes and riparian zones in a till mantled catchment. *Hydrological Processes*, *24*(16), 2222–2236. https://doi.org/10.1002/hyp.7656

Dingman, L. S. (2015). *Physical hydrology* (3rd ed.). Waveland Press, Inc.

Dodds, W. K., & Smith, V. H. (2016). Nitrogen, phosphorus, and eutrophication in streams. *Inland Waters*, *6*(2), 155–164. https://doi.org/10.5268/IW-6.2.909

Dunnette, P. V., Higuera, P. E., Mclauchlan, K. K., Derr, K. M., Briles, C. E., & Keefe, M. H. (2014). Biogeochemical impacts of wildfires over four millennia in a Rocky Mountain subalpine watershed. *New Phytologist*, *203*(3), 900–912. https://doi.org/10.1111/nph.12828

Eidenshink, J., Schwind, B., Brewer, K., Zhu, Z.-L., Quayle, B., & Howard, S. (2009). A project for monitoring trends in burn severity. *Fire Ecology*, *3*(1), 3–21. https://doi.org/10.4996/fireecology.0301003

Emelko, M. B., Silins, U., Bladon, K. D., & Stone, M. (2011). Implications of land disturbance on drinking water treatability in a changing climate: Demonstrating the need for "source water supply and protection" strategies. *Water Research*, *45*(2), 461–472. https://doi.org/10.1016/j.watres.2010.08.051

French, D. W., Schindler, D. E., Brennan, S. R., & Whited, D. (2020). Headwater catchments govern biogeochemistry in America's largest free-flowing river network. *Journal of Geophysical Research: Biogeosciences*, *125*(12), 1–20. https://doi.org/10.1029/2020JG005851

Ganio, L. M., Torgersen, C. E., & Gresswell, R. E. (2005). A geostatistical approach for describing spatial pattern in stream networks. *Frontiers in Ecology and the Environment*, *3*(3), 138–144.

Gardner, K. K., & McGlynn, B. L. (2009). Seasonality in spatial variability and influence of land use/land cover and watershed characteristics on stream water nitrate concentrations in a developing watershed in the Rocky Mountain West. *Water Resources Research*, *45*(8), 1–14. https://doi.org/10.1029/2008WR007029

Gomi, T., Sidle, R. C., & Richardson, J. S. (2002). Understanding processes and downstream linkages of headwater systems. *Bioscience*, *52*(10), 905–916. https://doi.org/10.1641/0006-3568(2002)052[0905:UPADLO]2.0.CO;2

Graham, R. T. (2003). *Hayman Fire case study*. Gen. Tech. Rep. RMRS-GTR-114. Retrieved from http://www.fs.fed.us/rm/hayman_fire/. https://doi.org/10.2737/RMRS-GTR-115

Hall, R. O., Sobota, D. J., Dodds, W. K., Findlay, S. E. G., Grimm, N. B., Hamilton, S. K., McDowell, W. H., O'Brien, J. M., Tank, J. L., Ashkenas, L. R., Cooper, L. W., Dahm, C. N., Gregory, S. V., Johnson, S. L., Meyer, J. L., Peterson, B. J., Poole, G. C., Valett, H. M., Webster, J. R., … Thomasn, S. M. (2009). Nitrate removal in stream ecosystems measured by 15N addition experiments: Denitrification. *Limnology and Oceanography*, *54*(3), 666–680. https://doi.org/10.4319/lo.2009.54.3.0666

Hall, S. (2017). *The legacy of Colorado's largest wildfire*. Denver Water.

Hesselbarth, M., Sciaini, M., With, K., Wiegand, K., & Nowosad, J. (2019). Landscapemetrics: An open-source R tool to calculate landscape metrics. *Ecography*, *42*, 1648–1657.

Huntington, J. L., Hegewisch, K. C., Daudert, B., Morton, C. G., Abatzoglou, J. T., McEvoy, D. J., & Erickson, T. (2017). Climate engine: Cloud computing and visualization of climate and remote sensing data for advanced natural resource monitoring and process understanding. *Bulletin of the American Meteorological Society*, *98*(11), 2397–2409. https://doi.org/10.1175/BAMS-D-15-00324.1

Isaak, D. J., Peterson, E. E., Ver Hoef, J. M., Wenger, S. J., Falke, J. A., Torgersen, C. E., Sowder, C., Steel, E. A., Fortin, M.-J., Jordan, C. E., Ruesch, A. S., Som, N., & Monestiez, P. (2014). Applications of spatial statistical network models to stream data. *Wiley Interdisciplinary Reviews: Water*, *1*(3), 277–294. https://doi.org/10.1002/wat2.1023

Jencso, K. G., McGlynn, B. L., Gooseff, M. N., Bencala, K. E., & Wondzell, S. M. (2010). Hillslope hydrologic connectivity controls riparian groundwater turnover: Implications of catchment structure for riparian buffering and stream water sources. *Water Resources Research*, *46*(10), 1–18. https://doi.org/10.1029/2009WR008818

Kattwinkel, M., & Szöcs, E. (2020). openSTARS: An Open Source Implementation of the "ArcGIS" Toolbox "STARS". R package version 1.2.2. Retrieved from https://cran.r-project.org/package=openSTARS

Lentile, L. B., Morgan, P., Hudak, A. T., Bobbitt, M., Lewis, S. A., Smith, A. M. S., & Robichaud, P. R. (2007). Post-fire burn severity and vegetation response following eight large wildfires across the Western United States. *Fire Ecology*, *3*(1), 91–108. https://doi.org/10.1227/01.NEU.0000089482.80879.9A

Likens, G. E., & Bormann, F. H. (1974). Linkages between terrestrial and aquatic ecosystems. *Bioscience*, *24*(8), 447–456. https://doi.org/10.2307/1296852

Likens, G. E., Bormann, F. H., Johnson, N. M., Fisher, D. W., & Pierce, R. S. (1970). Effects of forest cutting and herbicide treatment on nutrient budgets in the Hubbard Brook watershed-ecosystem. *Ecological Monographs*, *40*(1), 23–47. https://doi.org/10.2307/1942440

Lindsay, J. B. (2020). WhiteboxTools Version 1.4.0.

Lovett, G. M., Weathers, K. C., & Arthur, M. A. (2002). Control of nitrogen loss from forested watersheds by soil carbon:Nitrogen ratio and tree species composition. *Ecosystems*, *5*(7), 712–718. https://doi.org/10.1007/s10021-002-0153-1

Lowe, W. H., & Likens, G. E. (2005). Moving headwater streams to the head of the class. *Bioscience*, *55*(3), 196–197. https://doi.org/10.1641/0006-3568(2005)055[0196:MHSTTH]2.0.CO;2

McGuire, K. J., Torgersen, C. E., Likens, G. E., Buso, D. C., Lowe, W. H., & Bailey, S. W. (2014). Network analysis reveals multiscale controls on streamwater chemistry. *Proceedings of the National Academy of Sciences of the United States of America*, *111*(19), 7030–7035. https://doi.org/10.1073/pnas.1404820111

McManus, M. G., D'amico, E., Smith, E. M., Polinsky, R., Ackerman, J., & Tyler, K. (2020). Variation in stream network relationships and geospatial predictions of watershed conductivity. *Freshwater Science*, *39*(4), 704–721. https://doi.org/10.1086/710340

Morresi, D., Vitali, A., Urbinati, C., & Garbarino, M. (2019). Forest spectral recovery and regeneration dynamics in stand-replacing wildfires of central Apennines derived from Landsat time series. *Remote Sensing*, *11*(3), 1–18. https://doi.org/10.3390/rs11030308

Parsons, A., Robichaud, P. R., Lewis, S. A., Napper, C., & Clark, J. T. (2010). Field guide for mapping post-fire soil burn severity. In *Gen. Tech. Rep. RMRS-GTR-243*. https://doi.org/10.2737/RMRS-GTR-243

Peterson, E. E., & Ver Hoef, J. M. (2010). A mixed-model moving-average approach to geostatistical modeling in stream networks. *Ecology*, *91*(3), 644–651.

Peterson, E. E., & Ver Hoef, J. M. (2014). STARS: An ArcGIS toolset used to calculate the spatial information needed to fit spatial statistical models to stream network data. *Journal of Statistical Software*, *56*, 1–17.

Pickell, P. D., Hermosilla, T., Frazier, R. J., Coops, N. C., & Wulder, M. A. (2016). Forest recovery trends derived from Landsat time series for

North American boreal forests. *International Journal of Remote Sensing*, *37*(1), 138–149. https://doi.org/10.1080/2150704X.2015.1126375

Rhea, A. E., Covino, T. P., & Rhoades, C. C. (2021). Reduced N-limitation and increased in-stream productivity of autotrophic biofilms 5 and 15 years after severe wildfire. *Journal of Geophysical Research: Biogeosciences*, *126*(9), 1–16. https://doi.org/10.1029/2020JG006095

Rhoades, C. C., Chow, A. T., Covino, T. P., Fegel, T. S., Pierson, D. N., & Rhea, A. E. (2019). The legacy of a severe wildfire on stream nitrogen and carbon in headwater catchments. *Ecosystems*, *22*(3), 643–657. https://doi.org/10.1007/s10021-018-0293-6

Rhoades, C. C., Entwistle, D., & Butler, D. (2011). The influence of wildfire extent and severity on streamwater chemistry, sediment and temperature following the Hayman Fire, Colorado. *International Journal of Wildland Fire*, *20*(3), 430–442. https://doi.org/10.1071/WF09086

Rhoades, C. C., Nunes, J. P., Silins, U., & Doerr, S. H. (2019). The influence of wildfire on water quality and watershed processes: New insights and remaining challenges. *International Journal of Wildland Fire*, *28*(10), 721–725. https://doi.org/10.1071/WFv28n10_FO

Richer, E. E., Kampf, S. K., Fassnacht, S. R., & Moore, C. C. (2013). Spatiotemporal index for analyzing controls on snow climatology: Application in the Colorado Front Range. *Physical Geography*, *34*(2), 85–107. https://doi.org/10.1080/02723646.2013.787578

Robichaud, P., MacDonald, L., Freeouf, J., Neary, D., Martin, D., & Ashmun, L. (2003). Postfire rehabilitation of the Hayman Fire. In *Hayman Fire case study: USDA RMRS-GTR-114* (pp. 293–313). Retrieved from http://www.fs.fed.us/rm/pubs/rmrs_gtr114/rmrs_gtr114_293_314.pdf. https://doi.org/10.2737/RMRS-GTR-115

Rodríguez-González, P. M., García, C., Albuquerque, A., Monteiro-Henriques, T., Faria, C., Guimarães, J. B., Mendonça, D., Simões, F., Ferreira, M. T., Mendes, A., Matos, J., & Almeida, M. H. (2019). A spatial stream-network approach assists in managing the remnant genetic diversity of riparian forests. *Scientific Reports*, *9*(1), 1–10. https://doi.org/10.1038/s41598-019-43132-7

Ruleman, C. A., Bohannon, R. G., Bryant, Bruce, Shroba, R. R., & Premo, W. R. (2011). Geologic map of the Bailey 30′ × 60′ quadrangle, north-central Colorado: U.S. Geological Survey, Scientific Investigations Map SIM-3156, scale 1:100,000.

Rust, A. J., Hogue, T. S., Saxe, S., & McCray, J. (2018). Post-fire water-quality response in the western United States. *International Journal of Wildland Fire*, *27*(3), 203–216. https://doi.org/10.1071/WF17115

Rust, A. J., Saxe, S., McCray, J., Rhoades, C. C., & Hogue, T. S. (2019). Evaluating the factors responsible for post-fire water quality response in forests of the western USA. *International Journal of Wildland Fire*, *28*(10), 769–784. https://doi.org/10.1071/WF18191

Schroeder, T. A., Wulder, M. A., Healey, S. P., & Moisen, G. G. (2011). Mapping wildfire and clearcut harvest disturbances in boreal forests with Landsat time series data. *Remote Sensing of Environment*, *115*(6), 1421–1433. https://doi.org/10.1016/j.rse.2011.01.022

Seibert, J., & McGlynn, B. L. (2007). A new triangular multiple flow direction algorithm for computing upslope areas from gridded digital elevation models. *Water Resources Research*, *43*(4), 1–8. https://doi.org/10.1029/2006WR005128

Shogren, A. J., Zarnetske, J. P., Abbott, B. W., Iannucci, F., Medvedeff, A., Cairns, S., Duda, M. J., & Bowden, W. B. (2021). Arctic concentration–discharge relationships for dissolved organic carbon and nitrate vary with landscape and season. *Limnology and Oceanography*, *66*(S1), S197–S215. https://doi.org/10.1002/lno.11682

Smith, H. G., Sheridan, G. J., Lane, P. N. J., Nyman, P., & Haydon, S. (2011). Wildfire effects on water quality in forest catchments: A review with implications for water supply. *Journal of Hydrology*, *396*(1–2), 170–192. https://doi.org/10.1016/j.jhydrol.2010.10.043

Smithwick, E. A. H., Kashian, D. M., Ryan, M. G., & Turner, M. G. (2009). Long-term nitrogen storage and soil nitrogen availability in post-fire lodgepole pine ecosystems. *Ecosystems*, *12*(5), 792–806. https://doi.org/10.1007/s10021-009-9257-1

Stevens-Rumann, C. S., Kemp, K. B., Higuera, P. E., Harvey, B. J., Rother, M. T., Donato, D. C., Morgan, P., & Veblen, T. T. (2018). Evidence for declining forest resilience to wildfires under climate change. *Ecology Letters*, *21*(2), 243–252. https://doi.org/10.1111/ele.12889

Stevens-Rumann, C. S., & Morgan, P. (2019). Tree regeneration following wildfires in the western US: A review. *Fire Ecology*, *15*(1), 1–17. https://doi.org/10.1186/s42408-019-0032-1

Stream Solute Workshop. (1990). Concepts and methods for assessing solute dynamics in stream ecosystems. *Journal of the North American Benthological Society*, *9*(2), 95–119. https://doi.org/10.2307/1467445

Taylor, A. H., Poulos, H. M., Kluber, J., Issacs, R., Pawlikowski, N., & Barton, A. M. (2021). Controls on spatial patterns of wildfire severity and early post-fire vegetation development in an Arizona Sky Island, USA. *Landscape Ecology*, *36*(9), 2637–2656. https://doi.org/10.1007/s10980-021-01260-4

Tepley, A. J., Thompson, J. R., Epstein, H. E., & Anderson-Teixeira, K. J. (2017). Vulnerability to forest loss through altered postfire recovery dynamics in a warming climate in the Klamath Mountains. *Global Change Biology*, *23*(10), 4117–4132. https://doi.org/10.1111/gcb.13704

Turner, M. G., Smithwick, E. A. H., Metzger, K. L., Tinker, D. B., & Romme, W. H. (2007). Inorganic nitrogen availability after severe stand-replacing fire in the Greater Yellowstone ecosystem. *Proceedings of the National Academy of Sciences of the United States of America*, *104*(12), 4782–4789. https://doi.org/10.1073/pnas.0700180104

U.S. Geological Survey. (2018). 3D Elevation Program 10-Meter Resolution Digital Elevation Model. Retrieved from https://www.usgs.gov/core-science-systems/ngp/3dep/data-tools

Vannote, R., Minshall, G., Cummins, K., Sedell, J., & Cushing, C. (1980). The river continuum concept. *Canadian Journal of Fisheries and Aquatic Sciences*, *37*, 130–137.

Ver Hoef, J., & Peterson, E. (2020). SSN. R package version 1.1.15. Retrieved from https://cran.r-project.org/web/packages/SSN/SSN.pdf

Ver Hoef, J. M., Peterson, E. E., Cliord, D., & Shah, R. (2014). SSN: An R package for spatial statistical modeling on stream networks. *Journal of Statistical Software*, *56*(3), 1–45. https://doi.org/10.18637/jss.v056.i03

Vitousek, P. M., Gosz, J. R., Grier, C. C., Melillo, J. M., William, A., & Todd, R. L. (1979). Nitrate losses from disturbed ecosystems. *Science*, *204*(4392), 469–474.

Walker, R. B., Coop, J. D., Parks, S. A., & Trader, L. (2018). Fire regimes approaching historic norms reduce wildfire-facilitated conversion from forest to non-forest. *Ecosphere*, *9*(4), 1–17. https://doi.org/10.1002/ecs2.2182

Wan, S., Hui, D., & Luo, Y. (2001). Fire effects on nitrogen pools and dynamics in terrestrial ecosystems: A meta-analysis. *Ecological Applications*, *11*(5), 1349–1365. https://doi.org/10.1890/1051-0761(2001)011[1349:FEONPA]2.0.CO;2

Webster, J. R., & Valett, H. M. (2006). Solute dynamics. In *Methods in stream ecology* (2nd ed., pp. 169–185). Elsevier.

Westerling, A. L. R. (2016). Increasing western US forest wildfire activity: Sensitivity to changes in the timing of spring. *Philosophical Transactions of the Royal Society B: Biological Sciences*, *371*(1696), 940–943. https://doi.org/10.1098/rstb.2015.0178

Wilson, C., Kampf, S. K., Wagenbrenner, J. W., & MacDonald, L. H. (2018). Rainfall thresholds for post-fire runoff and sediment delivery from plot to watershed scales. *Forest Ecology and Management*, *430*(August), 346–356. https://doi.org/10.1016/j.foreco.2018.08.025

Wohl, E. (2017). The significance of small streams. *Frontiers of Earth Science*, *11*(3), 447–456. https://doi.org/10.1007/s11707-017-0647-y

WRCC. (2021). Daily Total Precipitation Cheesman, Colorado (Station 053102). Retrieved from https://wrcc.dri.edu/cgi-bin/rawMAIN.pl?coCCHE.

Wu, Q. (2021). whitebox: "WhiteboxTools" R Frontend. R package version 1.4.0. Retrieved from https://github.com/giswqs/whiteboxR

Zarnetske, J. P., Bouda, M., Abbott, B. W., Saiers, J., & Raymond, P. A. (2018). Generality of hydrologic transport limitation of watershed organic carbon flux across ecoregions of the United States. *Geophysical Research Letters*, *45*(21), 11702–11711. https://doi.org/10.1029/2018GL080005

Zimmerman, D. L., & Ver Hoef, J. M. (2017). The torgegram for fluvial variography: Characterizing spatial dependence on stream networks. *Journal of Computational and Graphical Statistics*, *26*(2), 253–264. https://doi.org/10.1080/10618600.2016.1247006

SUPPORTING INFORMATION

Additional supporting information can be found online in the Supporting Information section at the end of this article.

How to cite this article: Rhea, A. E., Covino, T. P., Rhoades, C. C., & Brooks, A. C. (2022). Use of geostatistical models to evaluate landscape and stream network controls on post-fire stream nitrate concentrations. *Hydrological Processes*, *36*(9), e14689. https://doi.org/10.1002/hyp.14689